K-, *L*-, and *M*-Shell Atomic Photoeffect for Screened-Potential Models*

R. D. SCHMICKLEY†
Lockheed Palo Alto Research Laboratory, Palo Alto, California

AND

R. H. PRATT‡
Department of Physics, University of Pittsburgh, Pittsburgh, Pennsylvania

(Received 17 July 1967)

Photoelectric cross sections for K through M_V subshells of iron, tin, and uranium have been numerically computed for x rays from 412 to 1332 keV using a relativistic multipole expansion of the matrix element. Electronic orbitals and partial waves were computed in the central-field approximation. Comparison of screened with unscreened results shows that angular distributions and polarization correlations are essentially unaffected by central-potential screening; total cross sections are merely renormalized by a factor equal to the square of the ratio of screened to Coulomb bound-state normalizations. This normalization effect is used to develop a table of realistic total cross sections for energies 10 to 3000 keV, and atoms $Z=13$ through 92. These predictions are compared with existing experimental data.

I. INTRODUCTION

THEORETICAL predictions for atomic photoelectric cross sections require the calculation of integrals over electron wave functions in the potential which represents the atom. In the relativistic region such calculations have usually been done numerically, beginning with the work of Hulme, McDougall, Buckingham, and Fowler[1] on K-shell total cross sections for a few point-Coulomb model atoms (i.e., no electron screening). Using modern electronic computers, these results have been extended by Hultberg, Nagel, and Olsson[2] and by Pratt, Levee, Pexton, and Aron.[3] Alling and Johnson[4] obtained L-shell Coulomb cross sections. More recently, cross sections in various screened potential models have been reported by Hall and Sullivan,[5] Matese and Johnson,[6] and Rakavy and Ron.[7]

This paper[8] is a report of further numerical calculations of photoelectric cross sections, following the methods of $P1$, undertaken to understand the effects of electron screening and the properties of emission from higher shells. In particular we have verified the argument that the only significant effect of electron screening comes from the change in normalization of the bound-state wave function[9]: Cross sections for two atomic models vary as the square of the corresponding bound-state normalizations. (This has the consequence that angular distributions and polarization correlations are essentially independent of screening.) This result has been established for each subshell K through M_V and for ranges of photon energy down to about twice the binding energy. We are thus able to compare with all previous work[1–7] and to utilize this "normalization effect" in constructing tables of total photoelectric cross sections, by shells, for realistic potential models in the range $Z\geq 13$ and 10 keV$<k<3$ MeV.

In Sec. II we summarize the mathematical formalism for these calculations, and in Sec. III we discuss our numerical methods. We do not attempt a complete presentation, referring the reader to $P1$, but rather give only as much of the theory and numerical methods as are needed to understand the new features in this work and to permit a discussion of our results. In Sec. IV we present the results we have obtained for total cross sections, differential cross sections, and polarization correlations. We use these data to demonstrate that screening is a normalization effect; with similar ideas we can also understand the relationships of cross sections from states of the same angular momentum. We then prepare tables of photoelectric cross sections and compare these with theory and experiment.

* Research supported in part by the Air Force Office of Scientific Research, Office of Aerospace Research, U. S. Air Force, under AFOSR Contract AF49(638)-1389, at Stanford University.
† Supported by the Lockheed Graduate Study Program at Stanford University, 1958–65.
‡ Supported in part by the U. S. Atomic Energy Commission under Contract No. AT(30-1)-3829.

[1] H. R. Hulme, J. McDougall, R. A. Buckingham, and R. H. Fowler, Proc. Roy. Soc. (London) **A149**, 131 (1935).
[2] S. Hultberg, B. Nagel, and P. Olsson, Arkiv Fysik **20**, 555 (1961); and to be published, hereafter referred to as HNO.
[3] R. H. Pratt, R. D. Levee, R. L. Pexton, and W. Aron, Phys. Rev. **134**, A898 (1964); **134**, A916 (1964). Hereafter we shall refer to these two papers as $P1$ and $P2$ respectively.
[4] W. R. Alling and W. R. Johnson, Phys. Rev. **139**, A1050 (1965).
[5] H. Hall and E. Sullivan, September, 1964 (private communication); Phys. Rev. **152**, 4 (1967).
[6] J. J. Matese and W. R. Johnson, Phys. Rev. **140**, A1 (1965).
[7] G. Rakavy and A. Ron, Phys. Letters **19**, 207 (1965); Phys. Rev. **159**, 50 (1967).
[8] A more complete account of this work can be found in R. D. Schmickley, Ph.D. dissertation, Stanford University, December, 1966 (unpublished).
[9] R. H. Pratt, Phys. Rev. **119**, 1619 (1960).

II. MATHEMATICAL FORMALISM

Following *P*1 we write the differential cross section for photoeffect as[10]

$$d\sigma/d\Omega=(2\pi)^{-2}p\epsilon|H|^2, \tag{2.1}$$

subject to energy conservation, where

$$H=(2\pi\alpha k^{-1})^{1/2}\int d^3r\,\psi_{\rm fin}{}^{\dagger}\boldsymbol{\alpha}\cdot\mathbf{e}\exp(i\mathbf{k}\cdot\mathbf{r})\psi_{\rm in}. \tag{2.2}$$

The initial electron wave is square normalized to unity, and the final wave is asymptotically normalized to a unit amplitude plane wave of 4-momentum $(\epsilon,\mathbf{p})$ plus an *incoming* spherical wave. The incident radiation is specified by 4-momentum $(k,\mathbf{k})$ and 4-polarization $(0,\mathbf{e})$. Both $\psi_{\rm fin}$ and $\psi_{\rm in}$ are solutions of the Dirac equation for a screened central potential.

The initial state is given by Eq. (2.10) in *P*1, and the final state by Eq. (2.16) in *P*1. With the exceptions that we use the phase shifts δ_l instead of δ_κ, and use K for the bound-state "kappa" quantum number, but with all other notation the same as in *P*1, we have

$$\psi_{\rm in}=\begin{pmatrix}G_{\rm K}(r)\Omega_{JLM}(\hat{r})\\ iF_{\rm K}(r)\Omega_{JL'M}(\hat{r})\end{pmatrix}, \tag{2.3}$$

and

$$\psi_{\rm fin}=4\pi\sum_{jlm}[\Omega_{jlm}{}^{\dagger}(\hat{p})U_A](i)^l e^{-i\delta_l}\begin{pmatrix}g_\kappa(r)\Omega_{jlm}(\hat{r})\\ if_\kappa(r)\Omega_{jl'm}(\hat{r})\end{pmatrix}. \tag{2.4}$$

We insert (2.3) and (2.4) into (2.2), and choosing the z axis along $\mathbf{k}$, we obtain[11]

$$H(M)=4\pi(i)^L(2\pi\alpha k^{-1})^{1/2}\times U_A{}^{\dagger}\left[e_+\begin{pmatrix}J_+(M)\\ K_+(M)\end{pmatrix}+e_-\begin{pmatrix}J_-(M)\\ K_-(M)\end{pmatrix}\right] \tag{2.5}$$

for $e_\pm=e_x\pm ie_y$. Here we have explicitly displayed the M dependence. The factor $(i)^L$ is a choice of the phase designed to give real integrals later on. The functions $J_\pm(M)$ and $K_\pm(M)$ are complex scalar functions which we call reaction amplitudes, after the definition of Nagel[12]; we will write them out explicitly later.

The cross section is obtained for definite M by putting (2.5) into (2.1). This gives bilinear products of $e_\pm$ and $e_\pm{}^*$, and also of the components of U_A and $U_A{}^{\dagger}$. These are combinations of the polarization parameters[13] ξ_i and ζ_j $(i,j=0,1,2,3)$, as defined in *P*1. The ξ_0 and ζ_0 are both unity and give the only contribution for unpolarized photon and electron beams respectively. The algebra yields

$$d\sigma(M)/d\Omega=(4\pi p\epsilon\alpha k^{-1})\sum_{ij}\xi_i\zeta_j\beta_{ij}(M), \tag{2.6}$$

where each of the sixteen $\beta_{ij}(M)$ is a bilinear function of the reaction amplitudes. Our interest here is in the cross section summed over all allowed values of M for the given subshell, so we sum Eq. (2.6) over all M from $-J$ to $+J$. Eight of the $\beta_{ij}(M)$ are even in M, and eight are odd; so upon summation we are left with only eight terms, which can be written as sums over positive M only:

$$d\sigma/d\Omega=(8\pi p\epsilon\alpha k^{-1})\sum_{ij}\xi_i\zeta_jB_{ij} \tag{2.7}$$

for

$$B_{ij}=\sum_{M=\frac{1}{2}}^{J}\beta_{ij}(M).$$

The eight nonzero B_{ij} are given explicitly in terms of the reaction amplitudes by Eqs. (2.25) in *P*1, where we understand that the right-hand side is to be summed over positive M. For example,

$$B_{00}=\sum_{M=\frac{1}{2}}^{J}[|J_-(M)|^2+|K_-(M)|^2+|J_+(M)|^2+|K_+(M)|^2].$$

The cross section (2.7) is for a general pair of photon-electron polarizations specified by the ξ_i, ζ_j. For the case of unpolarized photons and photoelectrons we average over incident photons and sum over final electrons to obtain

$$(d\sigma/d\Omega)_{\rm unpol}=(16\pi p\epsilon\alpha k^{-1})B_{00}. \tag{2.8}$$

We then rewrite (2.7) as

$$\frac{d\sigma}{d\Omega}=\left(\frac{d\sigma}{d\Omega}\right)_{\rm unpol}\tfrac{1}{2}\sum_{ij}\xi_i\zeta_jC_{ij}, \tag{2.9}$$

where the $C_{ij}(\equiv B_{ij}/B_{00})$ are called *polarization correlation* functions.

The cross sections are given in terms of the reaction amplitudes. We must write these amplitudes in terms of quadratures suitable for numerical computation. Carrying through the matrix multiplications and angular integrations we obtain

$$\begin{pmatrix}J_\pm(M)\\ K_\pm(M)\end{pmatrix}=\sum_\kappa e^{i\delta_l}R_\kappa{}^{\mp}(M)\Omega_{jlM\mp1}(\hat{p}), \tag{2.10}$$

where

$$R_\kappa{}^{\mp}(M)=\sum_{\nu=1}^{2}Q_\nu{}^{\mp}(\kappa,\mathrm{K},M)\times\sum_{\lambda}{}'P_\nu{}^{\mp}(\kappa,\mathrm{K},M;\lambda)S_\nu(\kappa,\mathrm{K};\lambda). \tag{2.11}$$

---

[10] We use the unrationalized "natural" unit system, $\hbar=m=c=1$. Hence $e^2=\alpha\approx1/137$. We shall also continue to use the notation of *P*1 and *P*2.

[11] We use the coordinate system of *P*1:

$$\hat{z}=\hat{k},\ \hat{y}=(\mathbf{k}\times\mathbf{p})|\mathbf{k}\times\mathbf{p}|^{-1},\ \hat{x}=\hat{y}\times\hat{z}.$$

[12] B. Nagel, Arkiv Fysik **18**, 1 (1960). In this work, and other works of HNO, the $\hat{z}$ axis is chosen along $\mathbf{p}$, not along $\mathbf{k}$. Thus, the *A*, *B*, *C*, *D* reaction amplitudes of HNO are related to our $J_\pm$, $K_\pm$ by a rotation transformation.

[13] The ξ_i are Stokes parameters of the photon polarization. The ζ_j define the direction of the electron spin *in its rest frame*.

The functions on the right-hand side of (2.11) are[14]:

$$Q_1^{\mp}(\kappa,\mathrm{K},M)=+\eta_\kappa(-1)^{M\mp\frac{1}{2}}[(2l'+1)(2L+1)]^{1/2}\times C_{jl'M\mp1}{}^{\mp}C_{JLM}{}^{\pm};$$

$$Q_2^{\mp}(\kappa,\mathrm{K},M)=-\eta_\mathrm{K}(-1)^{M\mp\frac{1}{2}}[(2l+1)(2L'+1)]^{1/2}\times C_{jlM\mp1}{}^{\mp}C_{JL'M}{}^{\pm};$$

$$P_1^{\mp}(\kappa,\mathrm{K},M;\lambda)=(i)^{l'+L-\lambda}(2\lambda+1)\times\begin{pmatrix} l' & L & \lambda \\ -M\pm\frac{1}{2} & M\mp\frac{1}{2} & 0\end{pmatrix}\times\begin{pmatrix} l' & L & \lambda \\ 0 & 0 & 0\end{pmatrix};$$

$$P_2^{\mp}(\kappa,\mathrm{K},M;\lambda)=(i)^{l+L'-\lambda}(2\lambda+1)\times\begin{pmatrix} l & L' & \lambda \\ -M\pm\frac{1}{2} & M\mp\frac{1}{2} & 0\end{pmatrix}\times\begin{pmatrix} l & L' & \lambda \\ 0 & 0 & 0\end{pmatrix};$$

$$S_1(\kappa,\mathrm{K};\lambda)=\int_0^\infty f_\kappa(r)G_\mathrm{K}(r)j_\lambda(kr)r^2dr;$$

$$S_2(\kappa,\mathrm{K};\lambda)=\int_0^\infty g_\kappa(r)F_\mathrm{K}(r)j_\lambda(kr)r^2dr. \qquad (2.12)$$

In (2.11) the summation over λ, denoted by $\sum'$, is carried from $\lambda_{\min}$ to $\lambda_{\max}$ *in steps of two*, where

$$\lambda_{\min}=\min[|l-L'|,|l'-L|],$$
$$\lambda_{\max}=\max[(l+L'),(l'+L)].$$

We point out four properties of the Eqs. (2.10) through (2.12): (1) The $R_\kappa^{\mp}(M)$ are real; (2) the spherical Bessel functions in the S integrals come from the multipole expansion of $\exp(i\mathbf{k}\cdot\mathbf{r})$; (3) the sum in (2.10) is over all $\kappa=\pm1,\pm2,\cdots$; (4) the R matrices of (2.11) and the reaction amplitudes of (2.10) reduce exactly to those in P1 when $\mathrm{K}=-1$, $M=\frac{1}{2}$ (i.e., for K shells).

Upon inserting (2.11) into the expression for $(d\sigma)_{\mathrm{unpol}}$, and integrating over $d\Omega(\hat{p})$, we obtain

$$\sigma_{\mathrm{unpol}}=(16\pi p\epsilon\alpha k^{-1})\times\sum_\kappa\sum_{M=\frac{1}{2}}^{J}[R_\kappa{}^{+}(M)^2+R_\kappa{}^{-}(M)^2], \qquad (2.13)$$

which agrees with $P1$ for K shells.

III. NUMERICAL METHODS

The problem of computing photoelectric cross sections has been reduced to computing the Q and P factors and S integrals of (2.12). The Q and P factors present no great problem. But the S integrals must be obtained by numerical integration of the threefold products of continuum wave functions, bound wave functions, and spherical Bessel functions.

Spherical Bessel functions were obtained with the method of Corbató and Uretsky.[15] The continuum and bound radial wave functions were obtained by numerical integration of the pair of equations:

$$\left(\frac{d}{dr}+\frac{1+\mathrm{K}}{r}\right)G_\mathrm{K}(r)-[E+1+\phi(r)]F_\mathrm{K}(r)=0;$$
$$\left(\frac{d}{dr}+\frac{1-\mathrm{K}}{r}\right)F_\mathrm{K}(r)+[E-1+\phi(r)]G_\mathrm{K}(r)=0. \qquad (3.1)$$

Equations (3.1) are written for the bound state ($E<1$). The same equations hold for the continuum state, except that we use $g_\kappa(r)$, $f_\kappa(r)$, κ, and $\epsilon(>1)$.

The function $\phi(r)$ is just $-V(r)$, where V is the screened central potential for the atomic electron in question. We have specified the screening by a factor $\chi(r)$, defined by

$$\phi(r)=(a/r)\chi(r) \qquad (3.2)$$

for $a\equiv Z\alpha$. In the present work we have made calculations for four different central potentials:

Coulomb, $\chi(r)\equiv1$; (3.3a)

Thomas-Fermi, $\chi(r)=\Phi(aqr)$, (3.3b)
for $q=2[4/(3\pi Z)]^{2/3}$,
and Φ, the "universal TF function"[16];

Kerner,[17] $\chi(r)=[1+1.525\alpha Z^{1/3}r]^{-1}$; (3.3c)

Yukawa, $\chi(r)=\exp(-\lambda r)$, (3.3d)
for $\lambda\approx1.12\alpha Z^{1/3}$.

Values of λ were taken from Matese and Johnson[6] in an effort to reproduce their results as a check of our program.

The bound states were computed from (3.1) with the methods developed in $P1$. However, we required that the relative variation of the *binding energy*, $\delta T/T$ (rather than of the *total energy*, $\delta E/E$) be small. This provides a more sensitive measure of deviations which is needed for the higher shells since the energy levels become too closely spaced if measured by E instead of $T(=1-E)$. Also, it was necessary to use Coulomb-like radial wave functions, which had the proper number of nodes, to start the iteration scheme. (In $P1$ only the nodeless K-shell functions were considered.) Finally, due to instabilities in the integration scheme, we im-

[14] The $C_{JLM}{}^{\pm}$ are the same as defined by Eq. (2.13) in $P1$ [However, there is a typographical error in that expression; the sign of C^{+} for $J=L-\frac{1}{2}$ should be $(-)$, not $(+)$.] The Ω_{JLM} are given by (2.12) in $P1$. The η_κ and η_K are the negative of the sign of the subscript (κ or K), as defined in $P1$.

[15] F. J. Corbató and J. L. Uretsky, J. Assoc. Comp. Mech. **6**, 366 (1959).

[16] We used Φ as given by V. Bush and S. Caldwell, Phys. Rev. **38**, 1898 (1931). A more accurate tabulation is given by S. Kobayashi, T. Matsukuma, S. Nogai, and K. Umeda, J. Phys. Soc. Japan **10**, 759 (1955).

[17] E. H. Kerner, Phys. Rev. **83**, 71 (1951).

posed a cutoff on the calculated functions at a radius of 1.5 to 3 times the classical turning radius. Beyond that point the functions were continued with their asymptotic approximations; the errors so induced in term values and wave functions (where they contribute to the integrals) are negligible.

The continuum functions were also computed with methods developed in P1, but with some important modifications. We first convert g_κ and f_κ to $\bar{g}_\kappa$ and $\bar{f}_\kappa$, which are finite at the origin:

$$\begin{aligned}\bar{g}_\kappa(r)&=r^{1-\gamma}g_\kappa(r)\,,\\ \bar{f}_\kappa(r)&=r^{1-\gamma}f_\kappa(r)\,,\end{aligned}\qquad(3.4)$$

for

$$\gamma=[\kappa^2-a^2]^{1/2}.$$

In $P1$ the first few points of $\bar{g}_\kappa$ and $\bar{f}_\kappa$ were obtained by a Taylor series expansion about the adjacent preceding point. [See Eq. (3.32) in $P1$.] However, we found it more satisfactory to expand each point about the origin. The coefficients of the expansion will of course depend upon the choice of potential $\phi(r)$. Although we used a different formula for each potential, we found that these differences cause insignificant deviations from expansions using the pure Coulomb potential. This is because near the nucleus the electron essentially sees a strong unscreened Coulomb potential.

The power series expansion was used for the first $2|\kappa|$ points, after which the integration was continued by the Runge-Kutta method.[18] Upon reaching the first minimum of $\bar{f}_\kappa(r)$, near $r=|\kappa|/p$, we switched from computing $\bar{g}_\kappa$ and $\bar{f}_\kappa$ to computing $\tilde{g}_\kappa$ and $\tilde{f}_\kappa$, defined by

$$\begin{aligned}\tilde{g}_\kappa(r)&=pr g_\kappa(r)\,,\\ \tilde{f}_\kappa(r)&=pr f_\kappa(r)\,.\end{aligned}\qquad(3.5)$$

It is desirable to do this because these new functions are asymptotically sinusoidal. The resulting numerical integration will always be within machine limits and thus requires no scaling factors as needed in $P1$.

The functions $\tilde{g}_\kappa(r)$ and $\tilde{f}_\kappa(r)$ are normalized with a method which generalizes that of $P1$. If we assume an approximate asymptotic form based upon a phase-shifted free-field solution,

$$\begin{aligned}\tilde{g}_\kappa(r)&\approx A_\kappa\left[\frac{\epsilon+1}{2\epsilon}\right]^{1/2} pr[\cos\delta_\kappa j_\kappa(pr)\\ &\qquad+(-1)^\kappa\sin\delta_\kappa j_{-\kappa-1}(pr)]\,,\\ \tilde{f}_\kappa(r)&\approx A_\kappa\left[\frac{\epsilon-1}{2\epsilon}\right]^{1/2} pr[\cos\delta_\kappa j_{\kappa-1}(pr)\\ &\qquad-(-1)^\kappa\sin\delta_\kappa j_{-\kappa}(pr)]\,,\end{aligned}\qquad(3.6)$$

where

$$\delta_\kappa\equiv\delta_l+(\kappa-l)\tfrac{1}{2}\pi\,,$$

then A_κ and δ_l (or δ_κ) are to be determined by matching the right-hand sides of (3.6) with the numerically computed $\tilde{g}_\kappa(r)$ and $\tilde{f}_\kappa(r)$ at some point r_0 in the free-field region of the atom. However, values of r for which the integration of $\tilde{g}_\kappa$ and $\tilde{f}_\kappa$ is feasible without excessive computation time are not sufficiently large: Applying (3.6) we do not get constants A_κ and δ_l, but some functions $A(r)$ and $\delta(r)$. Thus, a modification of (3.6) is needed.

We observe that in $P1$ the argument of the trigonometric functions in (3.6) was *not* just δ_κ, but was actually $(\delta_\kappa+\eta\ln 2pr)$, for $\eta=a\epsilon/p$. The distortion is due to persistence of the Coulomb potential. Similarly here, we change the argument to $[\delta_\kappa+Q(r)]$, where $Q(r)$ is yet to be determined. We now make the transformation

$$\tilde{g}_\kappa(r)=A(r)\left[\frac{\epsilon+1}{2\epsilon}\right]^{1/2}\sin[pr-\tfrac{1}{2}l\pi+\delta(r)+Q(r)]\,,$$

and similarly for $\tilde{f}_\kappa(r)$. Putting these into the equations for $\tilde{g}_\kappa(r)$ and $\tilde{f}_\kappa(r)$, we obtain equations for $A(r)$ and $\delta(r)$, and from these we deduce the asymptotic forms for $A(r)$ and $\delta(r)$:

$$\begin{aligned}&\ln A(r)\sim\kappa(2pr)^{-1}\sin 2pr+\text{const}\,;\\ &\delta(r)\sim\kappa(2pr)^{-1}\cos 2pr+\text{const}\\ &\qquad+(\epsilon/p)\int\phi(r)dr-Q(r)\,.\end{aligned}\qquad(3.7)$$

It is clear that we want $A(r)\to A_\kappa$ and $\delta(r)\to\delta_l$ as $r\to\infty$. So if we set the first constant to $\ln A_\kappa$, and the second to δ_l, then we see that for the Coulomb potential

$$Q(r)=-(\epsilon/p)\int_r^{(2p)^{-1}}\phi(s)ds=(a\epsilon/p)\ln 2pr\,,\qquad(3.8a)$$

and for screened potentials

$$Q(r)=-(\epsilon/p)\int_r^\infty\phi(s)ds\,.\qquad(3.8b)$$

With these choices $\ln A(r)$ oscillates about A_κ and $\delta(r)$ oscillates about δ_l, with amplitudes decreasing as r^{-1}, and periods π/p.

Thus if we use the approximate forms (3.6), but with $\delta_\kappa+Q(r)$ replacing δ_κ in the trigonometric functions, we can obtain A_κ and δ_l neglecting terms of $0[|\kappa|/(2pr_0)]$, where r_0 is the matching point. However, we can do even better if we average $A(r)$ and $\delta(r)$ over one (or more) period(s). Doing so reduces the errors to $0[|\kappa|/(4p^2r_0^2)]$. This averaging method was used in our present work.[19] We emphasize that $Q(r)$, which we call the *phase correction integral*, is extremely important, being of order 0.1 to 1 rad in most of our cases.

[18] See, for example, J. B. Scarborough, *Numerical Mathematical Analysis* (Johns Hopkins University Press, Baltimore, Maryland, 1958), 4th ed., p. 317.

[19] A more complete description of this method is found in Chap. 7 of Ref. 8.

Having obtained A_κ, we normalized our computed wave functions by dividing by it. These functions were then combined with the normalized bound-state waves and the spherical Bessel functions, and we numerically integrated the S integrals with Simpson's rule. In the present programs the integration grid was $\Delta r = 0.125/k$, so that Δkr was constant. This enabled us to use stored values of the $j_\lambda(kr)$ rather than compute these each time. The S integrals were combined with the Q and P factors to give R matrices, and these were combined to give amplitudes and cross sections.

We should finally discuss the accuracy of our numerical methods. Errors in the calculations of wave functions are discussed in $P1$, and present errors are of the same order, $\lesssim 10^{-4}$. Errors in Bessel functions, associated Legendre polynomials, 3-j symbols, etc. are completely negligible. The two major sources of error are (1) finite grid size in the S integration (histogram error), and (2) truncation error due to limitation of the number of κ's in the series (2.10) and (2.13).

To estimate the histogram errors in S integrals we made tests during the early stages of this work. Various grid sizes Δr ranging from 0.005 to 0.10 were used. The results generally fluctuated by 0(0.1%) for the grids tested; a few R matrices changed by $\approx 1\%$ when grid sizes or integration techniques were altered. We estimate that most of our integrations are accurate to $\lesssim 1\%$, probably $\approx 0.5\%$.

The other major source of error, truncation, can be tested by looking at the truncated sums σ_N, which are just the series (2.13) for κ running from $-N$ to $+N$. The truncation error is $1-\sigma_N/\sigma$. Plots of this truncation error decrease exponentially with N/p. This behavior can be used to predict the number of partial waves required to obtain a given accuracy for a specified momentum p. Computer storage/time requirements caused us to limit $|\kappa| \leq 20$. However, this was sufficient to calculate total cross sections with truncation error $\leq 0.1\%$, in most cases. A few high-energy higher shell calculations had truncation errors 0(0.5%). In the important regions of photoelectron emission the estimated truncation errors are 0(1%) for angular distributions and polarization correlations.

The combined effects of all errors are estimated to be $\leq 0.8\%$ for total cross sections, with most of these $<0.5\%$, and 0(1%) for angular distributions and polarization correlations.[20]

IV. RESULTS

A. Total Cross Sections

A separate numerical computation of the photoelectric cross section is necessary for each choice of photon energy, atomic number, subshell, and potential model. We present in Table I the total cross sections

[20] See further comments on errors in Chap. 10 of Ref. 8.

TABLE I. Total photoelectric cross sections in barns as computed in this work. Symbols C, TF, K, and Y refer to Coulomb, Thomas-Fermi, Kerner, and Yukawa potentials.

Shell	Z	keV	σ(C)	σ(TF)	σ(K)	σ(Y)
K	26	412	···	.239	···	···
	26	662	···	.0704	···	···
	26	1130	···	.0222	···	···
	47	279	···	···	···	10.4
	47	354	···	···	···	5.39
	50	412	4.73	4.56	···	···
	50	662	···	1.41	···	···
	50	1332	0.340	0.327	···	···
	92	412	59.9	58.5	58.9	···
	92	662	···	19.8	20.0	20.1
	92	1332	4.95	4.84	4.88	4.91
$L_{\rm I}$	26	412	0.0321	0.0211	···	···
	26	662	0.00949	0.00626	···	···
	26	1332	0.00219	···	···	···
	47	279	···	···	···	1.15
	47	354	···	···	···	0.598
	50	412	0.597	0.477	···	···
	50	662	0.186	0.149	···	···
	50	1332	0.0432	0.0346	···	···
	82	103	160.0	···	···	···
	82	279	13.0	···	···	···
	92	412	···	7.12	···	···
	92	662	···	2.45	···	···
	92	1332	0.668	···	0.601	0.631
$L_{\rm II}$	26	412	0.000625	0.000311	···	···
	26	662	0.000160	0.0000803	···	···
	26	1332	0.0000300	···	···	···
	47	279	···	···	···	0.0905
	47	354	···	···	···	0.0431
	50	412	0.0502	0.0352	···	···
	50	662	0.0138	0.00962	···	···
	50	1332	0.00275	0.00192	···	···
	92	412	···	2.89	···	···
	92	662	···	0.893	···	···
	92	1332	0.237	···	0.203	0.220
$L_{\rm III}$	26	412	0.000911	0.000444	···	···
	26	662	0.000243	0.000121	···	···
	47	279	···	···	···	0.108
	47	354	···	···	···	0.0505
	50	412	0.0565	0.0392	···	···
	50	662	0.0152	0.0106	···	···
	50	1332	0.00322	···	···	···
	92	412	···	1.64	···	···
	92	662	···	0.452	···	···
	92	1332	0.112	···	0.0924	0.102
$M_{\rm I}$	26	412	0.00952	0.00279	···	···
	50	412	···	0.0912	···	···
	50	662	···	0.0286	···	···
	92	412	···	1.61	···	···
	92	662	0.781	···	···	···
$M_{\rm II}$	26	412	0.000219	0.0000375	···	···
	50	412	···	0.00724	···	···
	50	662	···	0.00198	···	···
	92	412	···	0.700	···	···
	92	662	0.338	···	···	···
$M_{\rm III}$	26	412	0.000319	0.0000532	···	···
	50	412	···	0.00812	···	···
	50	662	···	0.00219	···	···
	92	412	···	0.428	···	···
	92	662	0.196	···	···	···
$M_{\rm IV}$	26	412	0.0000015	···	···	···
	50	412	···	0.0000702	···	···
	50	662	···	0.0000148	···	···
	92	412	···	0.0217	···	···
	92	662	0.0120	···	···	···
$M_{\rm V}$	26	412	0.0000020	···	···	···
	50	412	···	0.0000792	···	···
	50	662	···	0.0000190	···	···
	92	412	···	0.0193	···	···
	92	662	0.0110	···	···	···

TABLE II. Normalization effect error for Thomas-Fermi cross sections.

Subshell \ Z, keV	26 412	26 662	26 1332	50 412	50 662	50 1332	92 412	92 662	92 1332
K	−0.0076[a]	+0.0025[a]	−0.0028[a,b]	−0.0027	−0.0025	+0.0016	+0.0014	−0.0007[a]	−0.0008
L_{I}	+0.0084	+0.0042	···	−0.0024	−0.0043	−0.0047	−0.0175	−0.0131	···
L_{II}	+0.012	+0.0040	···	−0.0036	+0.0035	+0.0014	−0.0132[a]	−0.0143[a]	···
L_{III}	+0.0265	−0.0006	···	−0.0083	−0.0132	···	−0.0323[a]	−0.0145[a]	···
M_{I}	+0.0026	···	···	···	···	···	···	−0.0122[c]	···
M_{II}	+0.0048	···	···	···	···	···	···	−0.0172[c]	···
M_{III}	+0.0166	···	···	···	···	···	···	−0.0307[c]	···
M_{IV}	···	···	···	···	···	···	···	−0.0064[c]	···
M_{V}	···	···	···	···	···	···	···	−0.050[c]	···

[a] Coulomb cross sections taken from other sources.
[b] This point for 1130 keV.
[c] Thomas-Fermi cross sections from G. Rakavy and A. Ron.

in barns per atom obtained from about one hundred such computations, each taking about five minutes of computer time on Stanford's IBM-7090. We chose these cases to gain insight into the effects of central potential screening, to study the relationships of cross sections of various subshells, and to permit comparisons with previous calculations. We shall look at these three points in order; then we shall present tables of "realistic" cross sections which combine the theoretical results of this and other works.

In the absence of numerical results two approximate methods to take account of screening effects have been discussed. The best known method is to use the results for Coulomb cross sections, but everywhere replacing Z by $Z_{\mathrm{eff}}\equiv Z-s$, where s is a screening constant chosen to produce observed binding energies from the point Coulomb energy expression. It has been pointed out[9] that this "effective charge" method fits the atomic wave functions over the regions which give the main contribution to the normalization integral, but at least for energies well above threshold these are not the regions important for the photoeffect matrix element. Consequently the method is incorrect.

It has been argued[9] that for energies well above threshold screening is simply a "normalization effect." The reasoning is as follows. First, the main region of importance for the matrix element is the region of space where $r=0(1/\Delta)$, Δ being the minimum momentum transfer to the nucleus. For photon energies well above threshold, $\Delta=0(1)$. Second, the bound-state wave functions in the region $r=0(1)$ are in the field of the bare nuclear Coulomb potential and differ from exact Coulomb wave functions in normalization only, not in shape. Third, except at very low energies the continuum electron is not much affected (in shape or magnitude) by screening at distances $r=0(1)$, so the final state can be approximated by an exact Coulomb wave function. Similarly the shift in energy of ejected electrons due to the shift in binding energy for a screened bound state is negligible provided $\epsilon-1\gg a^2$. Thus the screened cross section should be proportional to the Coulomb cross section for the same photon energy, the constant of proportionality being the square of the ratio of screened to Coulomb bound-state normalization, *independent of energy*. This we call the *normalization effect* due to central potential screening.

We have used our data to test this argument. First define

$$\Xi=\lim_{r\to 0} G_{\mathrm{K}}^{s}(r)/G_{\mathrm{K}}^{c}(r)\,, \tag{4.1}$$

which is the ratio of screened (s) to Coulomb (C) bound-state normalizations for a given state K. If the normalization effect works, then the product $\Xi^2\sigma(\mathrm{C})/\sigma(s)$ should be unity. We define the normalization effect error $NE(s)$ by

$$NE(s)=\Xi^2\sigma(\mathrm{C})/\sigma(s)-1\,. \tag{4.2}$$

Using our data we computed this error for several cases, a few of which we show in Table II. These errors are of the order of computational errors, indicating that the effect works quite well for the Thomas-Fermi potential. Similar results were obtained for Kerner and Yukawa potentials.

In fact, the agreement is quite good even for energies of the order of a few times the binding energy. At these energies the continuum factor $p\epsilon$ in (2.1) can change by as much as 15% due to screening effects on the bound-state energy. The continued agreement with the normalization effect can be understood as follows. For very low energies, and at distances $r=0(1)$, the energy dependence of a continuum Coulomb wave function is[21] $(p\epsilon)^{-\frac{1}{2}}$, so $|H|^2$ varies as $(p\epsilon)^{-1}$. But this is exactly canceled by the factor $(p\epsilon)$ in Eq. (2.1). Hence, for low energies as well as high energies we get no variation in cross section due to the change in energy of the continuum wave. (It is known that for *given* p the normalization of a continuum wave is uneffected by screening down to very low energies.)

We conclude that it is possible to use Ξ^2 to account for screening over a wide range of photon energies. For example, using our values of Ξ^2, Alling and Johnson's[4] values of $\sigma(\mathrm{C})$, and Rakavy and Ron's[7] values of

[21] As $p\to 0$, the normalization (at $r=0$) goes as $[|\epsilon\kappa-\gamma|/p\epsilon]^{1/2}$. For $p\ll a/|\kappa|$ we neglect the variation of the numerator.

TABLE III. Normalization effect errors (NE) for low photon energies. Coulomb (C) data from Alling and Johnson; Thomas-Fermi (TF) data from Rakavy and Ron; normalizations from the present work. All data for $Z=92$.

Subshell	k (keV)	NE(TF)	$\frac{p\epsilon(\mathrm{TF})}{p\epsilon(\mathrm{C})}$
K	279	+0.0028	1.087
L_{I}	279	−0.0083	1.047
	103	−0.0015	1.116
	81	−0.0013	1.157
L_{II}	279	−0.0016	1.050
	103	−0.0005	1.123
	81	+0.0007	1.165
L_{III}	279	−0.0043	1.046
	103	−0.0020	1.111
	81	−0.0010	1.146

$\sigma(\mathrm{TF})$[22] we obtain the NE(TF) shown in Table III. Also listed are the factors $p\epsilon$. Even though this factor changes by 15% for 81 keV photons, the screening factor Ξ^2 gives correct results. So the normalization effect works for photon energies as low as 250 keV for the K shell of uranium (i.e., about 2×binding energy), and as low as 80 keV for the L subshells. Perhaps the method is valid at still lower energies, but present data is insufficient to test this. Similar results were obtained for the M shell and for lower Z.

These ideas can be extended to predict approximate ratios of cross sections for states having the same angular momentum K. This follows because in a given atom the wave functions of same K, but different n, are proportional in the important region $r=0(1)$, and the proportionality is independent of Z if relative $0(a^2)$ is neglected.[9] Thus, for example, the ratios of Coulomb cross sections from s states are given by the n-cubed rule,

$$\sigma(K):\sigma(L_I):\sigma(M_I):\sigma(N_I)=1:(1/8):(1/27):(1/64),$$

where relative $O(a^2)$ is neglected, independent of k. However, the Z dependence of $O(a^2)$ is not negligible in heavy elements, being 10% to 30% for uranium.[23] From the success of the normalization theory of screening, it is clear that these results will also hold in screened potentials: Present calculations indicate that the ratios of screened cross sections for same K are indeed *independent of* k to within 0(1%) over the energy range tested, 400 to 1300 keV.

With the normalization effect we are able to convert screened cross sections into Coulomb cross sections and *vice versa*, and so we can make comparisons with other calculations. We agree with the data of P1, HNO, Alling and Johnson, Hall and Sullivan, and Rakavy and Ron to within 0.8% for all points compared, with the exception of the L_I results for Coulomb potential, $Z=82$, $k=103$ keV. This energy is below the limit required for good accuracy of our program, so we suspect that Alling's result (153.9b) is better than ours. With this exception we are in excellent agreement with all these calculations. However, we do not agree with the results of Matese and Johnson,[6] as shown in Table IV, and we believe their results are incorrect. Matese and Johnson did not use a screened bound-state wave function, but instead used a Coulomb-like analytic function and varied some of the parameters until it gave the proper experimental binding energy. As with the Z_{eff} method this need not give the correct wave function in region of importance for the photoeffect, namely $r=0(1)$.

By combining previous work[2–5,7] with our present data, incorporating the normalization theory to fill in gaps and estimate higher shells, we have calculated a set of cross sections for a "realistic" screened potential. The "realistic" screened potential which we used is the relativistic Hartree-Fock-Slater potential computed by Liberman, Waber, and Cromer,[24] which we call the LWC potential. From their bound-state functions for the various subshells of several atoms we obtained values of Ξ^2. These ratios were multiplied by Coulomb cross sections, either calculated or interpolated, resulting in predictions of what would be obtained by direct calculation using the LWC model. We present results for the K shell in Table V, and for the total atom in Table VI. Not shown are similar results for L_I, L_{II}, L_{III}, L, M, and estimates for $N+0+\cdots$.[25] The data in Table V are believed accurate to $\lesssim 0.1\%$ for $Z\geq 20$, and $\approx 0.5\%$ for $Z=13$. Estimated errors for Table VI are $\lesssim 0.5\%$ for $Z\geq 20$ and $k\leq 1332$ keV. For $Z=13$ the errors may be 2%; for $k>1332$ keV the errors may be 1% to 2%.

TABLE IV. Comparison of Yukawa cross sections as calculated by Matese and Johnson (M&J) and the present authors (S&P).

Z	Subshell	k (keV)	σ (S&P) (barns)	σ (M&J) (barns)	$\frac{\sigma(\mathrm{S\&P})}{\sigma(\mathrm{M\&J})}$
47	K	279	10.38	10.21	1.0167
47	K	354	5.393	5.283	1.0208
47	L_{I}	279	1.155	0.9740	1.1858
47	L_{I}	354	0.5980	0.5100	1.1725
47	L_{II}	279	0.09047	0.0720	1.2565
47	L_{II}	354	0.04311	0.0340	1.2679
47	L_{III}	279	0.1077	0.093	1.1581
47	L_{III}	354	0.05046	0.044	1.1468
92	K	662	20.13	20.04	1.0045
92	K	1332	4.905	4.884	1.0043
92	L_{I}	1332	0.6307	0.6140	1.0272
92	L_{II}	1332	0.2195	0.2050	1.0707
92	L_{III}	1332	0.1015	0.0980	1.0357

[22] We use the notation: C=Coulomb; TF=Thomas-Fermi; K=Kerner; Y=Yukawa.

[23] For a more detailed discussion of this effect see Sec. 11.5 in Ref. 8.

[24] D. Liberman, J. T. Waber, and D. T. Cromer, Phys. Rev. **137**, A27 (1965). We wish to thank Dr. Liberman for kindly making available to us several listings of bound-state functions.

[25] A complete set of tables for all of these subshells and shells is given in Lockheed Rept. No. LMSC 5-10-67-11 Suppl. A, available in limited supply from the authors. All results are also in the dissertation, Ref. 8.

TABLE V. Theoretical photoelectric cross sections for K shells, in barns per atom.

Energy (keV)	Atomic number 13	20	26	29	42	47	50	60	74	78	79	82	84	92
10	1.02+03	5.49+03	1.38+04	1.94+04	0.00	0.00	0.00	0.00	0.00	0.00	0.00	0.00	0.00	0.00
20	1.24+02	7.30+02	2.02+03	3.06+03	0.00	0.00	0.00	0.00	0.00	0.00	0.00	0.00	0.00	0.00
30	3.51+01	2.20+02	6.39+02	9.78+02	3.66+03	5.34+03	6.66+03	0.00	0.00	0.00	0.00	0.00	0.00	0.00
40	1.41+01	9.26+01	2.75+02	4.28+02	1.68+03	2.53+03	3.16+03	0.00	0.00	0.00	0.00	0.00	0.00	0.00
50	6.95+00	4.69+01	1.41+02	2.22+02	9.17+02	1.39+03	1.75+03	3.43+03	0.00	0.00	0.00	0.00	0.00	0.00
60	3.86+00	2.65+01	8.09+01	1.28+02	5.54+02	8.45+02	1.06+03	2.04+03	0.00	0.00	0.00	0.00	0.00	0.00
70	2.35+00	1.62+01	5.03+01	8.01+01	3.58+02	5.47+02	6.86+02	1.32+03	2.62+03	0.00	0.00	0.00	0.00	0.00
80	1.53+00	1.06+01	3.33+01	5.32+01	2.41+02	3.74+02	4.71+02	9.12+02	1.85+03	2.27+03	0.00	0.00	0.00	0.00
90	1.04+00	7.34+00	2.32+01	3.72+01	1.72+02	2.66+02	3.36+02	6.58+02	1.37+03	1.65+03	1.69+03	1.89+03	0.00	0.00
100	7.42−01	5.27+00	1.68+01	2.70+01	1.26+02	1.97+02	2.49+02	4.92+02	1.05+03	1.24+03	1.29+03	1.45+03	1.59+03	0.00
125	3.59−01	2.62+00	8.47+00	1.36+01	6.52+01	1.02+02	1.31+02	2.65+02	5.78+02	6.90+02	7.25+02	8.12+02	8.83+02	1.15+03
150	2.00−01	1.48+00	4.83+00	7.84+00	3.81+01	6.05+01	7.78+01	1.60+02	3.53+02	4.25+02	4.44+02	5.04+02	5.47+02	7.31+02
175	1.23−01	9.21−01	3.02+00	4.88+00	2.41+01	3.87+01	4.96+01	1.04+02	2.30+02	2.82+02	2.93+02	3.35+02	3.65+02	4.93+02
200	8.17−02	6.13−01	2.01+00	3.27+00	1.64+01	2.63+01	3.40+01	7.14+01	1.62+02	1.97+02	2.06+02	2.36+02	2.58+02	3.52+02
279	2.94−02	2.23−01	7.41−01	1.22+00	6.26+00	1.02+01	1.33+01	2.85+01	6.66+01	8.17+01	8.59+01	9.89+01	1.08+02	1.52+02
300	2.36−02	1.79−01	5.99−01	9.85−01	5.09+00	8.30+00	1.08+01	2.34+01	5.48+01	6.76+01	7.11+01	8.21+01	9.01+01	1.27+02
354	1.43−02	1.10−01	3.72−01	6.14−01	3.23+00	5.27+00	6.88+00	1.49+01	3.55+01	4.41+01	4.64+01	5.39+01	5.93+01	8.41+01
400	1.00−02	7.74−02	2.64−01	4.37−01	2.32+00	3.79+00	4.96+00	1.09+01	2.62+01	3.25+01	3.42+01	3.98+01	4.39+01	6.27+01
412	9.21−03	7.12−02	2.45−01	4.05−01	2.14+00	3.51+00	4.61+00	1.01+01	2.43+01	3.02+01	3.18+01	3.70+01	4.08+01	5.85+01
500	5.43−03	4.19−02	1.45−01	2.40−01	1.29+00	2.12+00	2.79+00	6.19+00	1.52+01	1.89+01	1.99+01	2.32+01	2.57+01	3.72+01
600	3.38−03	2.65−02	9.13−02	1.52−01	8.21−01	1.36+00	1.78+00	3.99+00	9.86+00	1.23+01	1.30+01	1.52+01	1.69+01	2.46+01
662	2.68−03	2.13−02	7.23−02	1.20−01	6.47−01	1.07+00	1.41+00	3.17+00	7.88+00	9.88+00	1.04+01	1.22+01	1.35+01	1.99+01
700	2.37−03	1.87−02	6.34−02	1.05−01	5.71−01	9.46−01	1.25+00	2.80+00	6.98+00	8.75+00	9.24+00	1.08+01	1.20+01	1.76+01
800	1.75−03	1.37−02	4.68−02	7.74−02	4.22−01	6.99−01	9.23−01	2.07+00	5.19+00	6.53+00	6.90+00	8.11+00	8.99+00	1.33+01
900	1.35−03	1.05−02	3.61−02	5.99−02	3.27−01	5.44−01	7.17−01	1.62+00	4.06+00	5.11+00	5.39+00	6.34+00	7.04+00	1.04+01
1000	1.08−03	8.40−03	2.90−02	4.82−02	2.62−01	4.36−01	5.76−01	1.30+00	3.27+00	4.12+00	4.35+00	5.12+00	5.68+00	8.43+00
1131	8.45−04	6.61−03	2.27−02	3.77−02	2.05−01	3.42−01	4.51−01	1.01+00	2.56+00	3.22+00	3.41+00	4.01+00	4.46+00	6.62+00
1332	6.20−04	4.74−03	1.66−02	2.78−02	1.51−01	2.51−01	3.30−01	7.44−01	1.88+00	2.36+00	2.49+00	2.94+00	3.26+00	4.84+00
1500	5.01−04	3.89−03	1.34−02	2.24−02	1.22−01	2.02−01	2.66−01	5.99−01	1.51+00	1.90+00	2.00+00	2.36+00	2.62+00	3.89+00
2000	3.14−04	2.39−03	8.25−03	1.39−02	7.53−02	1.24−01	1.63−01	3.64−01	9.11−01	1.15+00	1.21+00	1.42+00	1.58+00	2.33+00
3000	1.76−04	1.35−03	4.60−03	7.60−03	4.03−02	6.63−02	8.71−02	1.92−01	4.76−01	5.95−01	6.29−01	7.37−01	8.16−01	1.20+00
4000	1.12−04	8.93−04	3.08−03	5.08−03	2.70−02	4.41−02	5.78−02	1.27−01	3.11−01	3.88−01	4.10−01	4.79−01	5.30−01	7.77−01
5000	8.16−05	6.72−04	2.32−03	3.81−03	2.00−02	3.27−02	4.28−02	9.38−02	2.28−01	2.84−01	2.99−01	3.50−01	3.87−01	5.66−01

TABLE VI. Theoretical photoelectric cross sections for complete atoms, in barns per atom.

Energy (keV)	Atomic number 13	20	26	29	42	47	50	60	74	78	79	82	84	92
10	1.10+03	6.02+03	1.56+04	2.22+04	1.31+04	2.07+04	2.66+04	5.46+04	3.08+04	3.85+04	4.05+04	4.67+04	5.12+04	6.86+04
20	1.34+02	8.01+02	2.26+03	3.44+03	1.87+03	3.02+03	3.93+03	8.41+03	1.98+04	2.42+04	2.55+04	2.94+04	3.22+04	2.70+04
30	3.78+01	2.41+02	7.11+02	1.09+03	4.25+03	6.31+03	7.91+03	2.76+03	6.65+03	8.25+03	8.67+03	1.00+04	1.10+04	1.55+04
40	1.53+01	1.01+02	3.06+02	4.76+02	1.94+03	2.96+03	3.71+03	1.23+03	3.03+03	3.77+03	3.97+03	4.65+03	5.11+03	7.31+03
50	7.49+00	5.14+01	1.57+02	2.47+02	1.05+03	1.61+03	2.04+03	4.08+03	1.63+03	2.05+03	2.17+03	2.53+03	2.80+03	4.06+03
60	4.16+00	2.90+01	8.97+01	1.42+02	6.33+02	9.76+02	1.24+03	2.43+03	9.86+02	1.24+03	1.31+03	1.54+03	1.71+03	2.49+03
70	2.53+00	1.78+01	5.58+01	8.92+01	4.08+02	6.30+02	7.96+02	1.57+03	3.26+03	8.12+02	8.59+02	1.01+03	1.12+03	1.65+03
80	1.65+00	1.17+01	3.69+01	5.92+01	2.75+02	4.30+02	5.45+02	1.08+03	2.29+03	2.83+03	5.92+02	6.99+02	7.75+02	1.15+03
90	1.12+00	8.06+00	2.57+01	4.14+01	1.96+02	3.06+02	3.89+02	7.80+02	1.69+03	2.05+03	2.11+03	2.39+03	5.60+02	8.35+02
100	8.00−01	5.78+00	1.87+01	3.01+01	1.43+02	2.26+02	2.88+02	5.82+02	1.28+03	1.54+03	1.61+03	1.83+03	2.01+03	6.27+02
125	3.87−01	2.87+00	9.39+00	1.52+01	7.41+01	1.18+02	1.51+02	3.12+02	7.04+02	8.52+02	8.96+02	1.01+03	1.11+03	1.49+03
150	2.15−01	1.62+00	5.36+00	8.72+00	4.33+01	6.94+01	8.97+01	1.88+02	4.28+02	5.22+02	5.48+02	6.27+02	6.85+02	9.41+02
175	1.33−01	1.01+00	3.35+00	5.44+00	2.74+01	4.44+01	5.72+01	1.22+02	2.80+02	3.46+02	3.61+02	4.15+02	4.55+02	6.31+02
200	8.81−02	6.72−01	2.23+00	3.64+00	1.86+01	3.01+01	3.02+01	8.38+01	1.96+02	2.41+02	2.53+02	2.92+02	3.20+02	4.49+02
279	3.17−02	2.45−01	8.23−01	1.35+00	7.11+00	1.16+01	1.53+01	3.34+01	8.03+01	9.95+01	1.05+02	1.22+02	1.34+02	1.92+02
300	2.54−02	1.97−01	6.65−01	1.10+00	5.79+00	9.52+00	1.25+01	2.74+01	6.61+01	8.22+01	8.66+01	1.01+02	1.11+02	1.60+02
354	1.54−02	1.21−01	4.13−01	6.84−01	3.67+00	6.04+00	7.92+00	1.75+01	4.28+01	5.35+01	5.65+01	6.61+01	7.31+01	1.06+02
400	1.08−02	8.51−02	2.94−01	4.87−01	2.63+00	4.34+00	5.71+00	1.27+01	3.15+01	3.94+01	4.16+01	4.87+01	5.39+01	7.89+01
412	9.93−03	7.82−02	2.72−01	4.51−01	2.43+00	4.02+00	5.30+00	1.18+01	2.92+01	3.66+01	3.86+01	4.53+01	5.02+01	7.36+01
500	5.85−03	4.61−02	1.61−01	2.68−01	1.46+00	2.43+00	3.21+00	7.23+00	1.82+01	2.28+01	2.41+01	2.84+01	3.15+01	4.66+01
600	3.65−03	2.91−02	1.02−01	1.69−01	9.35−01	1.56+00	2.06+00	4.66+00	1.18+01	1.49+01	1.58+01	1.86+01	2.06+01	3.08+01
662	2.90−03	2.34−02	8.04−02	1.33−01	7.35−01	1.23+00	1.63+00	3.70+00	9.44+00	1.19+01	1.26+01	1.49+01	1.66+01	2.48+01
700	2.55−03	2.05−02	7.05−02	1.17−01	6.49−01	1.08+00	1.43+00	3.27+00	8.35+00	1.06+01	1.12+01	1.32+01	1.47+01	2.20+01
800	1.89−03	1.50−02	5.20−02	8.62−02	4.80−01	8.02−01	1.06+00	2.42+00	6.22+00	7.88+00	8.34+00	9.86+00	1.10+01	1.65+01
900	1.46−03	1.16−02	4.02−02	6.68−02	3.72−01	6.23−01	8.26−01	1.89+00	4.85+00	6.15+00	6.50+00	7.69+00	8.58+00	1.30+01
1000	1.17−03	9.24−03	3.22−02	5.38−02	2.98−01	5.00−01	6.63−01	1.52+00	3.90+00	4.95+00	5.24+00	6.21+00	6.92+00	1.05+01
1131	9.14−04	7.26−03	2.52−02	4.20−02	2.33−01	3.91−01	5.18−01	1.18+00	3.05+00	3.88+00	4.11+00	4.86+00	5.42+00	8.21+00
1332	6.71−04	5.22−03	1.84−02	3.09−02	1.71−01	2.86−01	3.79−01	8.67−01	2.23+00	2.83+00	3.00+00	3.55+00	3.95+00	5.98+00
1500	5.42−04	4.28−03	1.49−02	2.50−02	1.38−01	2.30−01	3.05−01	6.97−01	1.79+00	2.27+00	2.41+00	2.85+00	3.18+00	4.79+00
2000	3.40−04	2.63−03	9.15−03	1.55−02	8.52−02	1.41−01	1.87−01	4.23−01	1.08+00	1.37+00	1.45+00	1.71+00	1.91+00	2.88+00
3000	1.89−04	1.48−03	5.09−03	8.44−03	4.57−02	7.56−02	9.97−02	2.24−01	5.66−01	7.13−01	7.55−01	8.88−01	9.88−01	1.48+00

TABLE VII. Comparisons of experimental total atomic photoeffect cross sections with predictions of the present work. Experimenters are (I) Titus, (II) Parthasaradhi *et al.*, (III) Latyshev, and (IV) Colgate.

Experimenter	Z	Photon (keV)	Exp. value (barns)	Predicted (barns)	Exp. value / Predicted
I	29	662	0.125±0.009	0.133	0.94±0.07
I	42	662	0.700±0.016	0.735	0.95±0.02
II	47	320	7.65 ±0.46	7.96	0.96±0.06
I	47	662	1.198±0.028	1.227	0.98±0.02
II	50	320	10.2 ±0.6	10.43	0.98±0.06
I	50	2620	0.11 ±0.03	0.123	0.89±0.27
I	73	662	8.55 ±0.14	8.90	0.96±0.02
I	73	2620	0.47 ±0.05	0.657	0.72±0.07
I	79	662	11.62 ±0.16	12.64	0.92±0.01
I	79	2620	0.74 ±0.06	0.926	0.80±0.06
II	82	320	76.5 ±4.6	85.6	0.89±0.05
III	82	2620	1.3 ±0.41	1.08	1.20±0.37
IV	92	412	73.2 ±0.2	73.5	1.00±0.00
IV	92	662	24.9 ±0.2	24.8	1.00±0.01
I	92	662	23.9[a]	24.8	0.96
IV	92	1332	5.9 ±0.1	5.98	0.99±0.02

[a] This figure was obtained by S. Hultberg from data of W. F. Titus, and appears in Arkiv Fysik **15**, 307 (1959).

In Table VII we compare our predictions for total atoms with the experiments of Titus,[26] Parthasaradhi *et al.*,[27] Latyshev,[28] and Colgate.[29] The data of Titus are consistently below the present calculations, usually not even within the stated limits of experimental error. The results of PLJ are in agreement with us for $Z=47$ and 50, but for $Z=82$ there is wide discrepancy. We agree quite well with Latyshev and with Colgate. In Table VIII we compare K-shell predictions with experiments of Missoni,[30] Seeman,[31] Bleeker *et al.*,[32] Latyshev,[28] and Hultberg and Stockendal.[33] The predicted values are always too small for the data of Seeman, Bleeker *et al.*, and Hultberg and Stockendal. It is not likely that our K-shell predictions could be too small while our total-atom predictions are too large, as would be the case if we accepted Titus's data as correct. Such a situation could be explained only if our predictions for higher shells were much too large. To see whether this could be the case we look at ratios $\sigma(K)/\sigma(L)$, $\sigma(K)/\sigma(M+\cdots)$, $\sigma(L)/\sigma(M+\cdots)$, and $\sigma(K+L+M+\cdots)/\sigma(K)$, which Hultberg[33] measured for uranium with photons between 412 and 1332 keV. He found nearly k-independent values of 5.3±0.2, 13.9±0.7, 2.6±0.15, and 1.26±0.01 respectively. Our predictions are 5.35±0.21, 16.9±1.2, 3.16±0.10, and 1.245±0.013. This indicates that our $M+\cdots$ contributions may be

TABLE VIII. Comparisons of experimental K-shell cross sections with predictions of the present work. Experimenters are (I) Missoni, (II) Seeman, (III) Bleeker *et al.*, (IV) Latyshev, and (V) Hultberg and Stockendal.

Experimenter	Z	Photon (keV)	Exp. value (barns)	Predicted (barns)	Exp. value / Predicted
I	79	662	10.2 ±0.03	10.44	0.98±0.03
II	82	511	23.4 ±0.7	22.06	1.06±0.03
III	82	1332	3.24±0.13	2.94	1.10±0.04
IV	82	2620	1.04±0.4[a]	1.09	0.95±0.4
III	82	2754	0.93±0.07	0.85	1.09±0.07
V	92	1172	7.2 ±0.5	6.16	1.17±0.08
V	92	1332	5.4 ±0.3	4.84	1.12±0.06

[a] This value was obtained by multiplying Latyshev's σ_A by his values of (σ_K/σ_A).

smaller than Hultberg's but our $\sigma(K)/\sigma(L)$ ratios are the same.

We know of no other direct measurements of absolute photoelectric cross sections. However, we can estimate "measured" cross sections by subtracting scattering (coherent and incoherent) from measurements of total x-ray attenuation. Wiedenbeck[34] measured attenuation in lead at 50, 105, 208, and 412 keV, yielding photoeffect components, by subtraction,[35] of 2335, 1484, 260, and 45.3 b, respectively. We predict 2531, 1606, 264, and 45.3 b. Agreement is good for the higher energies, but as K-shell threshold is approached the disagreement becomes 0(10%), due in part to inaccurate scattering cross sections near threshold. A similar analysis of the data of Deutch and Metzger[36] gives 113±3 b for 279-keV photons on gold. Our prediction is 116 b, in agreement. Finally, a few comparisons have been made with the recent compilation of experimental data by McMaster *et al.*[37] These comparisons indicate agreement of present theory with experiment to within 2% over a wide range of known cross sections.[38]

In addition to absolute cross sections we can compare relative cross sections and ratios for different states, atoms, or energies. Hultberg's experiment has already been discussed. Latyshev[28] gives K/A ratios[39] for $Z=73$ and $Z=82$ at 2.62 MeV; these are 0.815±0.035 and 0.80±0.035, respectively, to be compared with our values of 0.844 and 0.842. He also gets K/L ratios of 5.4 and 4.9, where we predict 6.5 and 6.0. These 20% discrepancies help to explain why our K/A ratios differ from his. Latyshev also measured the proportions $\sigma_A(Z=29):\sigma_A(Z=47):\sigma_A(Z=73):\sigma_A(Z=82)$ at 2.62 MeV, and he found them to be $(1\pm0.2):(9.5\pm1.1):$

[26] W. F. Titus, Phys. Rev. **115**, 351 (1959); Bull. Am. Phys. Soc. **4**, 269 (1958); Nucl. Phys. **69**, 179 (1965).
[27] K. Parthasaradhi V. Lakshminaryana, and S. Jnananda, Phys. Rev. **142**, 9 (1966). Hereafter we shall call this PLJ.
[28] G. D. Laytshev, Revs. Mod. Phys. **19**, 132 (1947).
[29] S. A. Colgate, Phys. Rev. **87**, 592 (1952).
[30] G. Missoni, Report ISS 65/11, Istituto Superiore di Sanita, Roma, Italy (unpublished).
[31] K. W. Seeman, Bull. Am. Phys. Soc. **1**, 198 (1956).
[32] E. J. Bleeker, P. F. A. Goudsmit, and C. De Vries, Nucl. Phys. **29**, 452 (1962).
[33] S. Hultberg and R. Stockendal, Arkiv Fysik **15**, 355 (1959).
[34] M. Wiedenbeck, Phys. Rev. **126**, 1009 (1962).
[35] We use scattering cross sections from G. W. Grodstein, U. S. Dept. of Commerce, NBS Circ. No. 583, 1957 (unpublished).
[36] B. I. Deutch and F. R. Metzger, Phys. Rev. **122**, 848 (1961).
[37] W. H. McMaster, N. Kerr Del Grande, J. H. Mallett, N. E. Scofield, R. Cahill, and J. H. Hubbell, University of California Lawrence Radiation Laboratory, Report No. UCRL-50174-II. 1967 (unpublished).
[38] W. H. McMaster, N. Kerr Del Grande, J. H. Mallett, N. E. Scofield, R. Cahill, and J. H. Hubbell, (private communication),
[39] Letter A represents total atomic cross section.

TABLE IX. Comparison of relative cross sections of Bergkvist versus present theory. These data are for $Z=79$, $k=412$ keV.

Function	Bergkvist	Present theory
σ_K/σ_L	5.7 ±0.4	6.11
σ_K/σ_{LI}	8.5 ±0.5	8.73
σ_{LII}/σ_{LI}	0.30±0.03	0.251
$\sigma_{LIII}/\sigma_{LI}$	0.18±0.02	0.179
$\frac{(\sigma_{LI}+\sigma_{LII})}{\sigma_{LIII}}$	7.2 ±0.8	6.97

(74±8):(120±11). Present theory predicts proportions of (1.12):(10.1):(72.1):(120), in good agreement. Several ratios have been experimentally determined by Grigor'ev and Zolotavin.[40] For example, they give K/L and K/A for 603 keV photons incident on Pt, these ratios being 0.058±0.005 and 0.818±0.02. Present theory predicts 0.062 and 0.827. Also their value of $(L_I+L_{II})/L_{III}$ for 265 keV photons on Bi is 5.0±0.5, and our prediction is 5.48. Bleeker *et al.*[32] have measured the K-shell cross section of Pb at 2754 keV compared to 1368 keV. They report a ratio of 0.30±0.02 as compared to our theoretical value of 0.304. A recent experiment by Bergkvist[41] has yielded cross section ratios for gold at 412 keV. These are summarized in Table IX. Agreement with our theory is again excellent. We conclude that to the extent that experimental results are consistent we are in agreement with them. There seems to be no reason to question present theory until the experimental situation is clarified. For now, our tables should provide a satisfactory tabulation of photoeffect cross sections in the ranges indicated.

B. Angular Distributions and Polarization Correlations

We define normalized angular distributions as $\sigma^{-1}(d\sigma/d\Omega)_{\text{unpol}}$. These were computed for each of the hundred cases listed in Table I.[42] If screening is a normalization effect, we expect that the normalized angular distribution should be essentially unaffected by screening. Significant deviations of screened from unscreened results were seen only for extreme angles, low energies, and high shells. Analytic comparisons were made by computing rms deviations of shape between the several screened results and the Coulomb results. These rms errors were 0(2%) for 412 keV, 0(1%) for 662 keV, and 0(0.5%) for 1332 keV. Thus, the normalized angular distributions are not much affected by central potential screening. In the following discussion we shall not specify the potentials since all

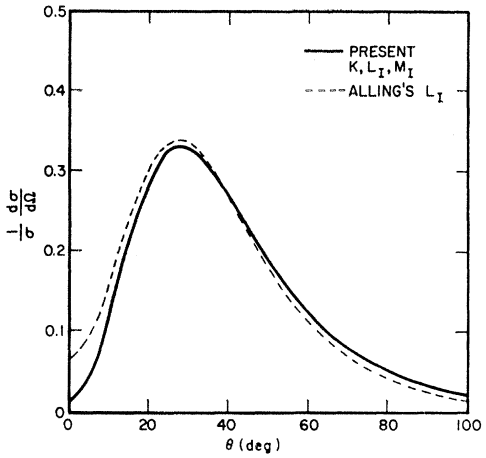

FIG. 1. Normalized photoelectron angular distributions for K, L_I, and M_I subshells of uranium for 412-keV incident radiation.

give essentially the same results. In Figs. 1 and 2 we show typical examples of these shapes, all computed for $Z=92$ and $k=412$ keV. In Fig. 1 the K, L_I, and M_I are essentially coincident—a manifestation of the normalization effect for subshells of same K. The L_{II} and M_{II} shapes in Fig. 2 are the same for $\theta>20°$, but differ slightly for $\theta<20°$. We see similar behavior for L_{III} and M_{III} subshells, but with somewhat greater deviations from coincidence. The saddle in the M_{IV} shape seems to be a real effect which was computed for several cases.

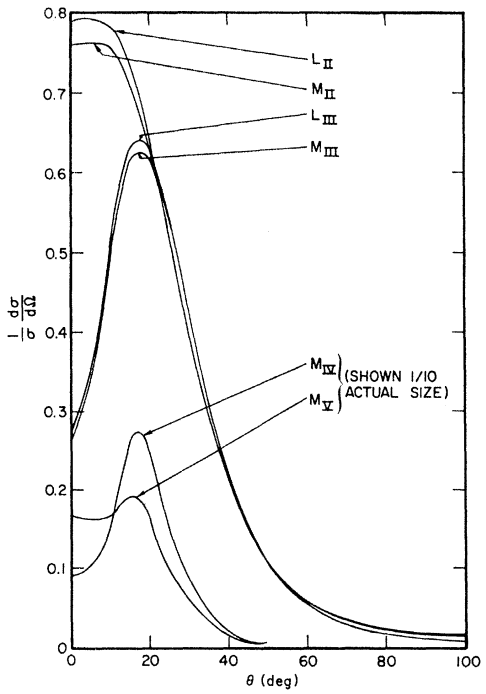

FIG. 2. Normalized photoelectron angular distributions for L_{II}, L_{III}, M_{II}, M_{III}, M_{IV}, and M_V subshells of uranium for 412-keV incident radiation.

[40] E. P. Grigor'ev and A. V. Zolotavin, Zh. Eksperim. i Teor. Fiz. **36**, 393 (1959) [English transl.: Soviet Phys.—JETP **9**, 272 (1959)].

[41] K. E. Bergkvist, Arkiv Fysik **27**, 483 (1964).

[42] Complete tables of calculated angular distributions and polarization correlations are given in Appendix E of Ref. 8, and in Lockheed Report No. LMSC 5-10-67-12, available in limited supply from the authors.

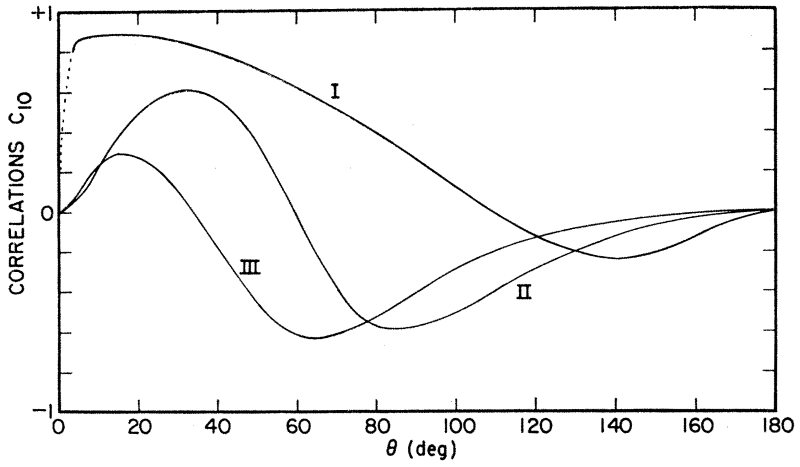

FIG. 3. Polarization correlations C_{10} for s, $p_{1/2}$, and $p_{3/2}$ subshells of tin for 412-keV incident radiation.

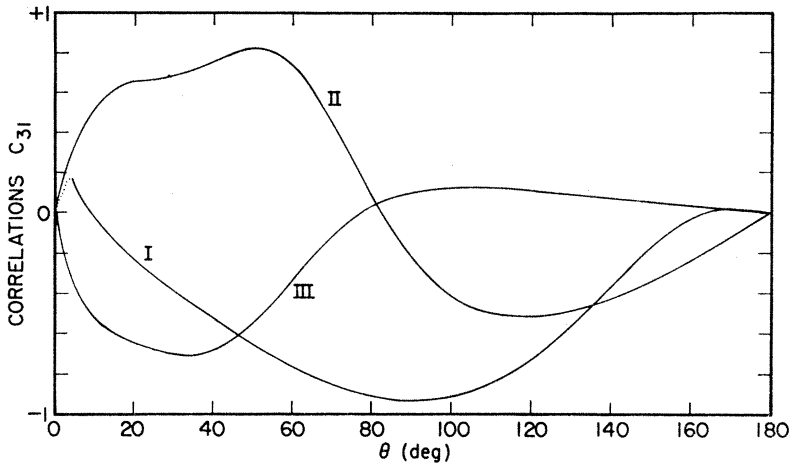

FIG. 4. Polarization correlations C_{31} for s, $p_{1/2}$, and $p_{3/2}$ subshells of tin for 412-keV incident radiation.

The angular distributions computed in the present work can be compared with a few sample calculations by others. Our K-shell distributions are identical with those of $P1$ and HNO. However, we disagree with the L-shell distributions of Alling and Johnson.[4] For example, the dotted line in Fig. 1 indicates their result for L_I, and it is obvious that there is a systematic difference between curves.[43] In view of our agreement with $P1$ and HNO, and the agreement, as expected, between K and L_I, we believe that Alling's distributions are slightly in error. However, his total cross sections are correct.

We cannot directly compare our distributions with experment, since our choices of Z and k are not found in any published experimental study of distributions, but we can point out indirect comparisons. Experimental work on uranium by Sujkowski[44] compares well with K-shell predictions of HNO, considering the difficulties involved in unfolding the true angular distributions from the raw data. Bergkvist's[45] K-shell distributions for gold are in excellent agreement with HNO, and his L_I distributions are the same as his K distributions, in agreement with our results.[46] Most of these measurements are limited by experimental problems to $\theta > 20°$. We conclude that the available experimental angular distributions show excellent agreement with the theory for $\theta > 20°$. Extreme forward distributions are not known well enough experimentally to make reliable comparisons.

There are only two sources in the current literature with which we can compare our polarization correlations. These are the numerically computed correlations of HNO and $P2$.[3] Both of these sources calculate the correlations for K shells only. Experimentally, there have been investigations of the azimuthal asymmetry of unpolarized photoelectrons from plane-polarized photons,[47] from which one could obtain C_{10};

[43] An early version of Alling and Johnson's article contained a K distribution for uranium at 412 keV which did not agree with $P1$, HNO, or the present work, nor was it the same distribution that was later published. This indicates that they discovered an error in that particular case, and suggests that some of their other distributions may be incorrect.

[44] Z. Sujkowski, Arkiv Fysik **20**, 269 (1961).

[45] K. E. Bergkvist, (Ref. 41); see also, K. E. Bergkvist and S. Hultberg, Arkiv Fysik **27**, 321 (1964).

[46] For more detail on these comparisons, see Chap. 12 of Ref. 8.

[47] L. W. Fagg and S. S. Hanna, Rev. Mod. Phys. **31**, 711 (1959), pages 724–5.

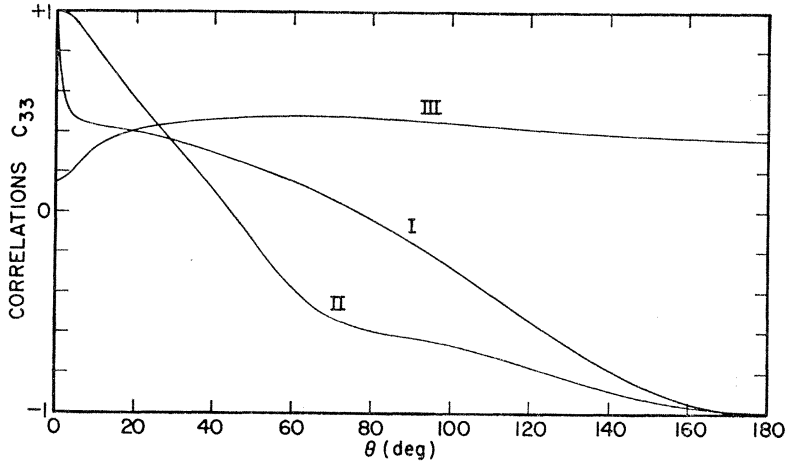

FIG. 5. Polarization correlations C_{33} for s, $p_{1/2}$, and $p_{3/2}$ subshells of tin for 412-keV incident radiation.

however, the data is contradictory. Other correlations have not been investigated experimentally.

It is generally true of all of the present K-shell correlations that they agree extremely well with both HNO and $P2$. In addition the correlations for a given Z, k, n, and K were the same when computed for different central potentials; i.e., they are independent of screening. In general the correlations for states of the same angular momentum K were essentially identical for $10°<\theta<120°$; slight deviations were noticed for $\theta<10°$ or $\theta>120°$, but these could not be measured experimentally with present techniques. Thus, it appears that the normalization effect is valid for polarization correlations in the main regions of photoelectric emission.

The preceding facts allow us to make simplifying generalizations in a presentation of the data. We shall label the states of different angular momentum by I, II, III corresponding to s states (K, L_I, M_I), $p_{1/2}$ states (L_{II}, M_{II}), and $p_{3/2}$ states (L_{III}, M_{III}). One plot of each C_{ij} can represent all subshells of angular momentum I, or II, or III. No distinction need be made between screened or unscreened calculations.

Only a few representative graphs are presented to indicate the shapes of some of these functions. Other graphs and tables of such functions can be found in HNO, $P2$, and Ref. 8. We show C_{10} in Fig. 3, C_{31} in Fig. 4, and C_{33} in Fig. 5, all for 412 keV x rays on tin. The physical meaning of these and other correlations is discussed in $P2$ and Ref. 8. We only mention that C_{10} measures photoeffect from linearly polarized photons, C_{31} measures the production of transversely polarized photoelectrons with circularly polarized photons, and C_{33} governs the transfer of helicity from photons to photoelectrons. For bound states with $J=\frac{1}{2}$ this must be $+1$ at $\theta=0$, but for $J\geq\frac{3}{2}$ it is not unity, indicating incomplete forward helicity transfer for states of higher angular momentum.

ACKNOWLEDGMENTS

We wish to thank Frank Bates and Don Gold, of the staff of the Stanford Computation Center, who generously provided several necessary support routines for our computer programs. Special thanks for unpublished material are extended to Dr. Solve Hultberg, Dr. Akiva Ron, Dr. Harvey Hall, Dr. William McMaster, Nancy Kerr Del Grande, and especially to John H. Hubbell.